

Optimizing tissue clearing and imaging methods for human brain tissue

Journal of International Medical Research

49(3) 1–17

© The Author(s) 2021



Article reuse guidelines:

sagepub.com/journals-permissions

DOI: 10.1177/03000605211001729

journals.sagepub.com/home/imr



Min Sun Kim^{1,*}, Jang Ho Ahn^{1,*} , Ji Eun Mo¹,
Ha Young Song¹, Deokhyeon Cheon¹,
Seong Ho Yoo² and Hyung Jin Choi^{1,3,4,5} 

Abstract

Objectives: To identify optimum sample conditions for human brains, we compared the clearing efficiency, antibody staining efficiency, and artifacts between fresh and cadaver samples.

Methods: Fresh and cadaver samples were cleared using X-CLARITYTM. Clearing efficiency and artifact levels were calculated using ImageJ, and antibody staining efficiency was evaluated after confocal microscopy imaging. Three staining methods were compared: 4-day staining (4DS), 11-day staining (11DS), and 4-day staining with a commercial kit (4DS-C). The optimum staining method was then selected by evaluating staining time, depth, method complexity, contamination, and cost.

Results: Fresh samples outperformed cadaver samples in terms of the time and quality of clearing, artifacts, and 4',6-diamidino-2-phenylindole (DAPI) staining efficiency, but had a glial fibrillary acidic protein (GFAP) staining efficiency that was similar to that of cadaver samples. The penetration depth and DAPI staining improved in fresh samples as the incubation period lengthened. 4DS-C was the best method, with the deepest penetration. Human brain images containing blood vessels, cell nuclei, and astrocytes were visualized three-dimensionally. The chemical dye staining depth reached 800 μm and immunostaining depth exceeded 200 μm in 4 days.

Conclusions: We present optimized sample preparation and staining protocols for the visualization of three-dimensional macrostructure in the human brain.

¹Functional Neuroanatomy of Metabolism Regulation Laboratory, Department of Anatomy, Seoul National University College of Medicine, Seoul, South Korea

²Institute of Forensic Medicine and Department of Forensic Medicine, Seoul National University College of Medicine, Seoul, South Korea

³BK21Plus Biomedical Science Project Team, Seoul National University College of Medicine, Seoul, South Korea

⁴Wide River Institute of Immunology, Seoul National University, Hongcheon, South Korea

⁵Neuroscience Research Institute, Seoul National University College of Medicine, Seoul, South Korea

*These authors contributed equally to this work.

Corresponding author:

Hyung Jin Choi, Seoul National University College of Medicine, 101 Daehak-ro, Jongno-gu, Seoul 03080, South Korea.

Email: hjchoi@snu.ac.kr



Keywords

Tissue clearing, human brain, X-CLARITY™, confocal microscopy, GFAP staining, DAPI staining

Date received: 4 February 2021; accepted: 16 February 2021

Introduction

To improve the diagnosis and treatment of various degenerative diseases that are unique to humans, it is important to perform studies using human brains. However, studies using human brains have lagged behind those using rodents and non-human primates because of the ethical, legal, and accessibility challenges of obtaining human brains. In recent years, there have been substantial improvements in the techniques used to visualize rodent brains in three dimensions (3D) without the use of tissue sectioning.¹⁻⁷ These techniques include various tissue-clearing technologies as well as advances in confocal microscopy that allow images to be taken from deep inside the brain.^{2,8-10} For example, iDISCO+ (immunolabeling-enabled three-dimensional imaging of solvent-cleared organs) has been used to image the vasculature of the adult mouse brain,¹¹ FDISCO (three-dimensional imaging of solvent-cleared organs with superior fluorescence-preserving capability) has been used to visualize neurons with weak fluorescence labeling in the whole mouse brain,¹² and MACS (m-xylylenediamine-based aqueous clearing system) has enabled the clearing of whole mouse brains with robust lipophilic dye compatibility.¹³ Among the tissue-clearing techniques, CLARITY (Clear, Lipid-exchanged, Acrylamide-hybridized, Rigid, Imaging/immunostaining compatible, Tissue hYdrogel) is a novel method in which formaldehyde-fixed tissues are infiltrated with hydrogel to form crosslinked biomolecules, thus forming a stable tissue

structure. This is followed by the extraction of lipid molecules using electrophoretic tissue clearing.^{1,14} The tissue obtains a lower refractive index once lipids have been removed, and the structural damage is minimal, with protein loss of only about 10%.¹⁵ Although this process allows the relatively deep diffusion of antibodies and other labeling probes,¹⁶ challenges remain for the antibody staining of large tissue samples and/or human samples. Most of the research into CLARITY has been conducted using fixed rodent brain tissue.⁹

Despite these challenges, a few recent studies have applied tissue-clearing techniques to the human brain to investigate the human dysplastic brain¹⁷ and the pathogenesis of Alzheimer's disease,^{8,18} Lewy body disease,¹⁹ and autism¹⁴ in 3D. Other studies have compared different tissue-clearing technologies for the human brain,²⁰ and have optimized the CLARITY procedure and immunofluorescence labeling in formalin-fixed brain tissue.^{21,22} A new permeabilization method, SHANEL (small-micelle-mediated human organ efficient clearing and labeling), was used in another study to render the human brain transparent.²³ Although most of these studies were conducted on cadaver samples, a few studies used both 'recently autopsied' (fresh) and cadaver samples.^{2,19} However, these studies did not quantitatively compare the clearing time, artifacts (including autofluorescence and scattered fluorescence), and staining efficiency between fresh and cadaver samples.² In addition, only a few studies compared a range of methods of antibody

staining, which is often considered the major bottleneck in human brain tissue clearing research.²⁴ Thus, to date, there is no established method for clearing and imaging macrostructures in human brain samples.

Our aim was to determine the optimal sample selection and staining strategy to visualize structures in cleared human brain samples. We therefore compared clearing efficiency, artifact levels, and antibody staining efficiency between donated cadaver samples and fresh samples. Furthermore, a range of staining methods were compared and evaluated according to staining time, staining depth, complexity of the method, tissue contamination, and cost. Our results provide an optimized protocol for 3D histological investigations in the human brain.

Materials and methods

Acquisition and storage of human brain samples

The collection and analysis of autopsied human specimens was approved by the Institutional Review Board for Human Subjects Research, and was carried out by a certified staff member of the Department of Forensic Medicine of Seoul National University (Seoul, South Korea) using the standard operating procedure for

conducting autopsies. The studies involving human participants were reviewed and approved by the Institutional Review Board of Seoul National University Hospital. Written informed consent for participation was not required for this study in accordance with national legislation and institutional requirements. No potentially identifiable human images or data are presented in this study.

All eight autopsied cortex samples were collected within 80 hours postmortem. The autopsied samples were stored at 4°C between death and sample collection. After the autopsies, the following information was collected from the Department of Forensic Medicine of Seoul National University: sex, age at death, height, weight, cause of death, and estimated postmortem interval (PMI) (Table 1). A portion around the central sulcus of the cortex from each individual was fixed in 4% paraformaldehyde (PFA) at 4°C for 1 week before being stored in phosphate-buffered saline (PBS) solution with 0.02% sodium azide.

The cadaver brain tissue samples (Table 2) were donated by the Department of Anatomy at Seoul National University College of Medicine. Brain cortex tissue blocks from the cadavers were stored in 4% PFA at 4°C for more than 1 year. Tissue blocks were immersed in PBS

Table 1. Clinical information from the fresh samples.

Fresh sample ID	Age (approximate)	Height (cm)	Weight (kg)	Cause of death	Postmortem interval (hours)
F1	41–45	179	86	CKD	30
F2	76–80	162	52	MI	48
F3	56–60	171	66	Hypothermia	48
F4	–	–	–	–	–
F5	61–65	173	66	MI	80
F6	66–70	166	70	Drowning	72
F7	26–30	163	48	Arrhythmia	70
F8	61–65	166	68	Hypertension	48

CKD, chronic kidney disease; MI, myocardial infarction.

Table 2. Clinical information from the cadaver samples.

Cadaver number	Year of birth	Year of death	Cause of death
C1	1932	2016	Myelodysplastic syndrome
C2	1951	2016	Angina pectoris
C3	1944	2016	Colon cancer
C4	1940	2016	Lung cancer
C5	1941	2016	Cardiac arrest
C6	1935	2016	Acute cardiac death
C7	1946	2016	Multiple organ failure
C8	1939	2016	Myasthenia gravis

solution with 0.02% sodium azide before undergoing any experimental procedures.

Tissue clearing

The tissue blocks were manually sectioned (approximately 1 mm thick) using razor blades and were incubated in hydrogel for 1 day. For the fresh samples, the initial samples (F4, F5, F8) were crudely sectioned with more than 1-mm thickness, whereas the latter samples (F1, F2, F3) were precisely sectioned at 1-mm thickness using a 1-mm lattice. The polymerization process was then performed for 3 hours using the X-CLARITY™ Polymerization System (−90 kPa; LOGOS Biosystems, Anyang, South Korea). The tissue blocks were then washed with PBS for 3 hours and were cleared using X-CLARITY™. The fresh and cadaver brain samples were cleared until the last intact sample was chemically disintegrated (30 hours for fresh, 50 hours for cadaver).

Immunofluorescence and chemical dye staining

Three different types of staining methods were applied. The first method was “4-day staining” (4DS). Pre-processed samples were incubated in primary antibody solution comprising anti-gial fibrillary acidic protein (GFAP) antibody (dilution 1:500, ab7260; Abcam, Cambridge, UK) in

0.02% sodium azide in PBS for 4 days. They were then washed in PBS for 2 days, incubated in secondary antibody solution comprising anti-rabbit 488 nm (dilution 1:250, A-11008; Invitrogen, Carlsbad, CA, USA), 4',6-diamidino-2-phenylindole (DAPI; dilution 1:1000, D1306, Invitrogen), and lectin (dilution 1:500, DL-1177; Vector Laboratories, Burlingame, CA, USA) in 0.02% sodium azide in PBS for 4 days, and washed in PBS for 2 days. The second method was “11-day staining” (11DS). Each step was the same as that described for the 4DS protocol, except the incubations with the primary and secondary antibodies were for 11 days each. The third method was “4-day staining with a commercial kit” (4DS-C), in which the DeepLabel Kit (C33001; LOGOS Biosystems) was used. Brain tissue samples were first immersed in permeabilization buffer for 2 days. Next, the samples were incubated in primary antibody solution containing anti-GFAP antibody (dilution 1:500, ab7260; Abcam) in DeepLabel Kit staining buffer for 4 days, and were then washed in PBS for 2 days. The samples were then incubated in secondary antibody solution containing anti-rabbit 488 nm (dilution 1:250, A-11008; Invitrogen), DAPI (dilution 1:1000, D1306; Invitrogen), and lectin (dilution 1:500, DL-1177; Vector Laboratories) in DeepLabel Kit staining buffer for 4 days, and were washed in PBS for 2 days.

Image acquisition and data analysis

The imaging of stained tissue was performed using an LSM 800 confocal microscope (Carl Zeiss Meditec, Oberkochen, Germany) at the Cancer Research Institute in Seoul National University, and a TCS ST8 confocal microscope (Leica Microsystems, Wetzlar, Germany). After staining, the samples were submerged in mounting solution for 4 hours for the homogenization of the refractive index. Images were then acquired with the confocal microscope using laser excitation wavelengths of 405 nm, 488 nm, and 594 nm. A 10× objective (working distance 200–500 μm, imaging interval 0.9–2.0 μm) and a 20× objective (working distance 200 μm, imaging interval 2.0 μm) were used. The staining depth was quantified as the *z*-axis depth of the shallowest *xy*-plane image that did not contain any signal except artifacts. The *z*-axis interval between the adjacent *xy*-plane image was 2 μm.

Image visualization was performed using Zen Blue (Carl Zeiss Meditec) and LAS X (Leica Microsystems) software. The 3D renderings were obtained using Zen Blue, LAS X, and Imaris (Bitplane, Belfast, UK) software.

Calculating tissue opacity

The opacity of the cleared samples was evaluated using ImageJ software (National Institutes of Health, Bethesda, MD, USA). The images of samples were trimmed to 1 cm × 0.8 cm rectangles before clearing and after clearing. The raw opacity of each rectangle was estimated as the closed area of the gel profile plot (with *x*-axis indicating the *x* coordinate and *y*-axis indicating the relative density of the contents per unit length) shown from the gel analyzer in ImageJ. The percentage opacity was then calculated as follows: Raw opacity of the sample after clearing/raw

opacity of the sample before clearing. The percentage opacity of each sample was regarded as the clearing efficiency of the sample.

Calculating artifacts, amount of stained antigens, and DAPI staining efficiency

Artifacts caused by autofluorescence and laser scattering phenomena in individual samples were assumed to be proportional to the image brightness when projected with a 405 nm, 488 nm, and 594 nm laser. The brightness after laser projections was quantified as the integrated density (“IntDen”) value in ImageJ, which is the product of signal intensity (mean gray value) and the area of the signal. The integrated density values of the image under each laser wavelength were added as the final artifact level. The amount of stained antigen in each sample was assumed to be proportional to the brightness of the fluorescence emitted from the GFAP antibodies of each sample after 4DS. The brightness of the GFAP signal was also quantified as the integrated density value of each sample. The DAPI staining efficiency of individual samples was assumed to be proportional to the brightness of the DAPI signal. The brightness of the DAPI signal was also quantified as the integrated density value of each sample.

Results

Clearing efficiency in fresh and cadaver samples

Using X-CLARITY™, the clearing efficiency (i.e., transparency) steadily increased (i.e., the opacity decreased) in a non-linear trajectory as the clearing time increased (Figure 1a). Eighty-percent transparency (i.e., 20% opacity) was obtained after an average of 4 hours for the fresh samples and 40 hours for the cadaver samples

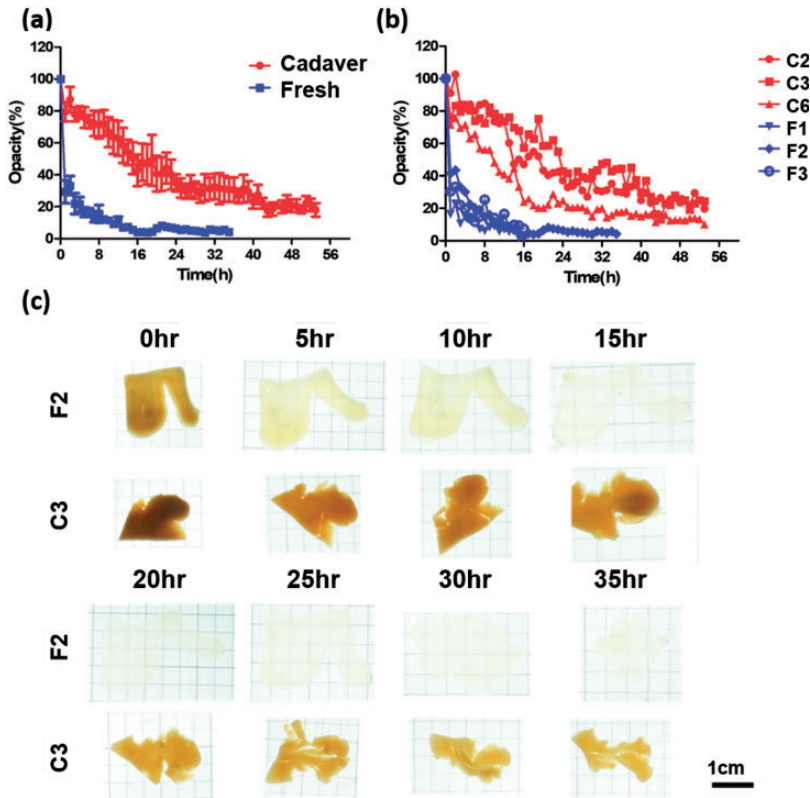


Figure 1. Clearing efficiency of the fresh and cadaver samples. (a) Graph of the mean clearing efficiency of fresh ($n = 3$) and cadaver ($n = 3$) samples over time. (b) Individual graphs of the clearing efficiencies of fresh (F1, F2, F3) and cadaver (C2, C3, C6) samples over time. (c) Images of fresh (F2) and cadaver (C3) samples at different clearing times.

(Figure 1a). This time difference between the two groups was statistically significant (two-tailed independent t -test, $p = 0.006$). The threshold opacity was set to 20% because of tissue dissociation and the fluctuating opacity values of fresh samples below 20% opacity (Figure 1b). Both the fresh and cadaver samples showed swelling after clearing. In addition, a yellowish stain in the cadaver samples remained even after clearing (Figure 1c). Taken together, these results indicate that fresh samples outperform cadaver samples in terms of the time and quality of clearing efficiency.

Artifact levels in fresh and cadaver samples

Artifacts caused by autofluorescence and laser scattering phenomena can interfere with fluorescence image acquisition. When the degree of artifacts was compared between cadaver and fresh samples that had been cleared for 14 hours, the cadaver samples had more apparent artifacts (Figure 2a). Moreover, the distribution of artifacts was more scattered in cadaver samples compared with fresh samples (Figure 2b) when the clearing efficiency was set to 20% opacity for both sample

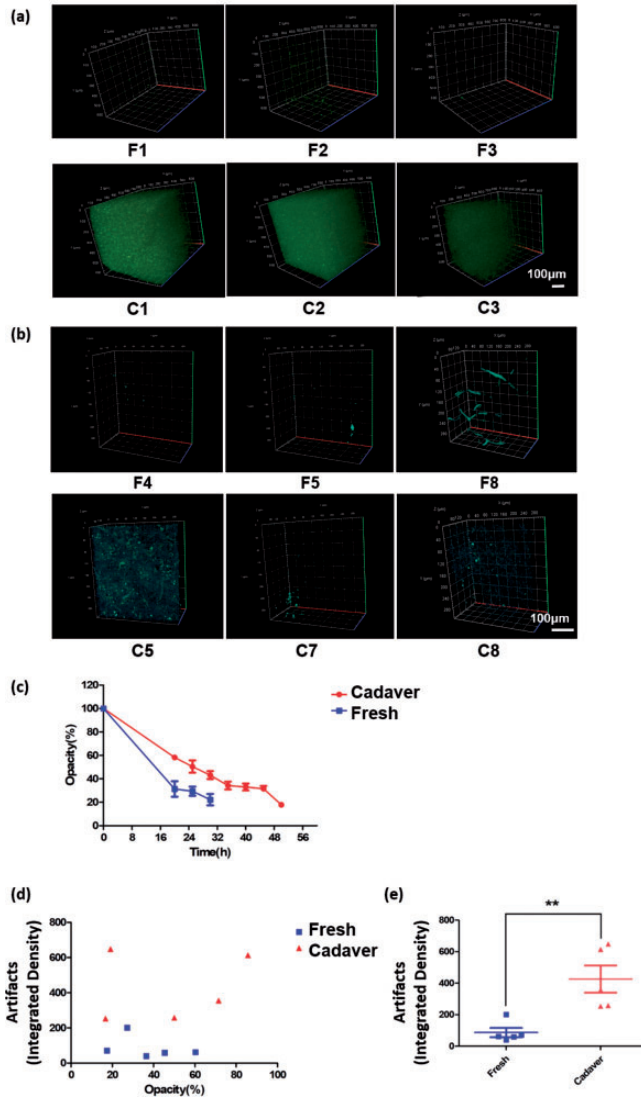


Figure 2. Artifact levels of fresh and cadaver samples. (a) Artifacts in fresh (F1, F2, F3) and cadaver (C1, C2, C3) samples. All images were taken with a confocal microscope (LSM 800); laser wavelength: 561 nm (green), 0.2%; 488 nm (red), 0.18%; detector gain: 700 V; detector digital gain: 2.0. (b) Artifacts in fresh (F4, F5, F8) and cadaver (C5, C7, C8) samples. All images were taken with a confocal microscope (LSM 800); laser wavelength: 561 nm, 0.2% (green); 488 nm, 0.2% (red); 405 nm, 0.14% (blue); detector gain: 750 V; detector digital gain: 1.0. (c) Transparency based on the clearing time of fresh (F4, F5, F8) and cadaver (C5, C7, C8) samples. (d) Integrated density based on opacity. (e) Artifact levels (as integrated density) compared between fresh and cadaver samples ($p = 0.004$). $**p < 0.01$.

types, which was achieved by setting different clearing times (Figure 2c). We then quantified the artifact levels in samples as the integrated density in ImageJ software.

Artifacts were proportional to opacity in fresh samples only ($r = -0.38$ and 0.17 for fresh and cadaver samples, respectively) (Figure 2d). Even within a similar opacity

range, all cadaver samples had a higher number of artifacts compared with the fresh samples (Figure 2d). In addition, the overall number of artifacts in the cadaver samples was significantly higher than that of the fresh samples ($p < 0.05$) (Figure 2e). Thus, our findings suggest that fresh samples have less artifacts than cadaver samples.

Staining efficiency in fresh and cadaver samples

Three staining methods were compared: 4DS, 11DS, and 4DS-C. To compare the staining efficiencies of fresh and cadaver samples, we first stained the cleared tissue samples according to the 4DS protocol, using DAPI and an anti-GFAP antibody.

The 1-mm slices of cadaver tissue samples showed no DAPI staining (only auto-fluorescence) after 4 days of staining (Figure 3a). Furthermore, no DAPI staining was observed in this tissue even when 30 μm sections were used. In contrast, fresh samples showed definite DAPI staining in the 3D cleared 30- μm sections (Figure 3b). GFAP staining was similarly good in both fresh and cadaver samples under the same clearing time of 20 hours (Figure 3c), or under the same clearing efficiency (Figure 3d).

We then measured the depth of GFAP staining to quantitatively evaluate these results. The difference in depth between the fresh (67.86 μm) and cadaver (65.85 μm) samples was not statistically significant (two-tailed independent t -test) (Figure 3e).

Together, these results suggest that DAPI staining is more efficient in fresh samples, whereas GFAP staining efficiency is similar between fresh and cadaver samples (Table 3).

Relationship between the PMI and the amount of stained antigen in fresh human brain samples

There was high heterogeneity in the amount of stained antigen among samples.

We speculated that the PMI may be an important determinant of the amount of stained antigen. However, although there was a trend toward a negative correlation between the PMI and the amount of stained antigen ($r = r^2 0.3557$), this was not statistically significant (t -test) (Figure 4).

Penetration depth of DAPI staining in fresh human brain samples

DAPI is a nanoscale chemical dye that efficiently penetrates tissue to stain nucleic acids. However, the exact depth of DAPI staining achieved with different incubation periods has not been studied precisely in human brain samples. We stained the human cerebral cortex with DAPI for varying lengths of time (1, 2, 4, 8, 16, and 32 hours) and revealed that when DAPI incubations lasted over 16 hours, DNA staining was achieved at a depth of over 500 μm (Figure 5a). Because the intensity of the laser is lower and the brightness of the fluorescence is not uniform when images are captured deeper within the tissue, the depth comparisons were achieved by post-processing the images for optimum brightness and contrast. We also confirmed that not only the depth of staining, but also the fluorescence brightness of the sample surface, were improved by a longer incubation time (Figure 5b). For a more quantitative comparison, the integrated density value was calculated for each depth ($z = 0, 10, 50,$ and $100 \mu\text{m}$) and each incubation period (1, 2, 4, 8, 16, and 32 hours) using ImageJ. The cross-sectional images for each depth were captured using the confocal microscope z -stack function. The integrated density values by depth and incubation period were then visualized as a heatmap (Figure 5c).

Comparison of staining methods in fresh human brain samples

We compared the staining time, antibody penetration depth, method complexity,

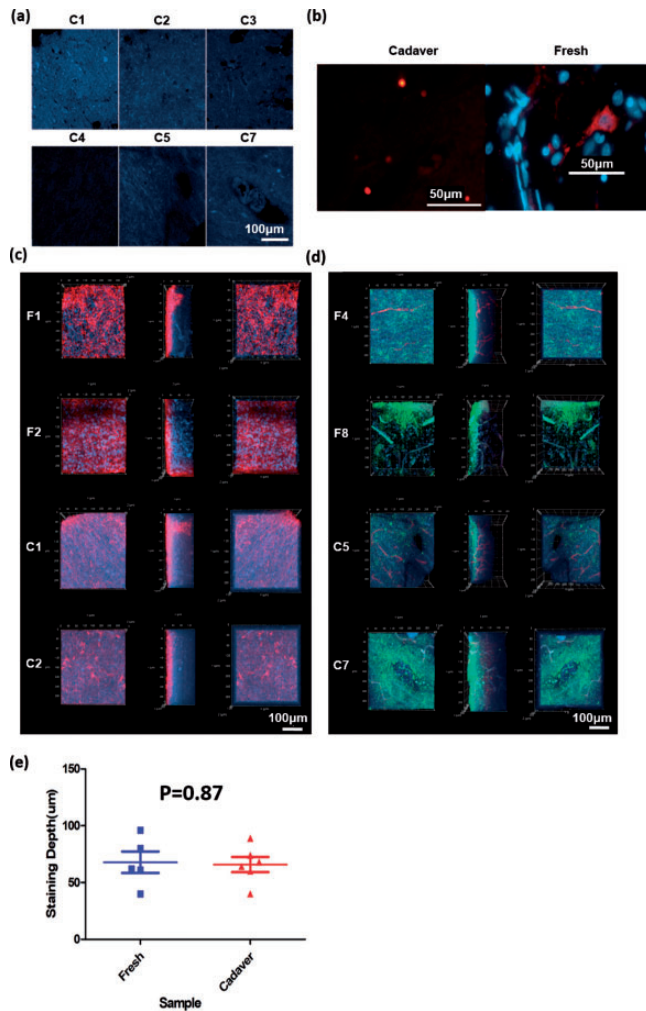


Figure 3. Staining efficiencies of fresh and cadaver samples. (a) 4',6-Diamidino-2-phenylindole (DAPI) staining results of 1 mm slices from cadaver samples (C1, C2, C3, C4, C5, C7) (b) Sectioned image of 30 μm sections from fresh and cadaver samples. (c) 4-day staining results from fresh (F1, F2) and cadaver (C1, C2) samples in three dimension (3D), all with a clearing time of 20 hours (red: glial fibrillary acidic protein [GFAP], blue: DAPI). (d) 4-day staining results from fresh (F4, F8) and cadaver (C5, C7) samples in 3D with the same clearing efficiency (red: lectin, green: GFAP, blue: DAPI). (e) Depth of GFAP staining in fresh and cadaver samples.

level of tissue contamination, and cost of the 4DS, 11DS, and 4DS-C antibody staining methods using fresh brain samples (Table 4, Table 5, Figure 6a). The 4DS-C method achieved deeper antibody staining than the 4DS or 11DS methods (4DS-C:

161 μm vs. 4DS: 68 μm vs. 11DS: 126 μm, $p=0.007$, analysis of variance), and the difference in depth between the 4DS and 4DS-C samples remained significant after a Bonferroni *post-hoc* analysis ($p=0.031$) (Figure 6b–d). In contrast, the differences

Table 3. Comparison of the fresh and cadaver samples.

	Fresh	Cadaver
Clearing time (average until 20% opacity)	4 hours	40 hours
Artifacts	Low	High
Antibody penetration depth (mean)	67.86 μm	65.85 μm
DAPI staining	Sufficient	Insufficient

DAPI, 4',6-diamidino-2-phenylindole.

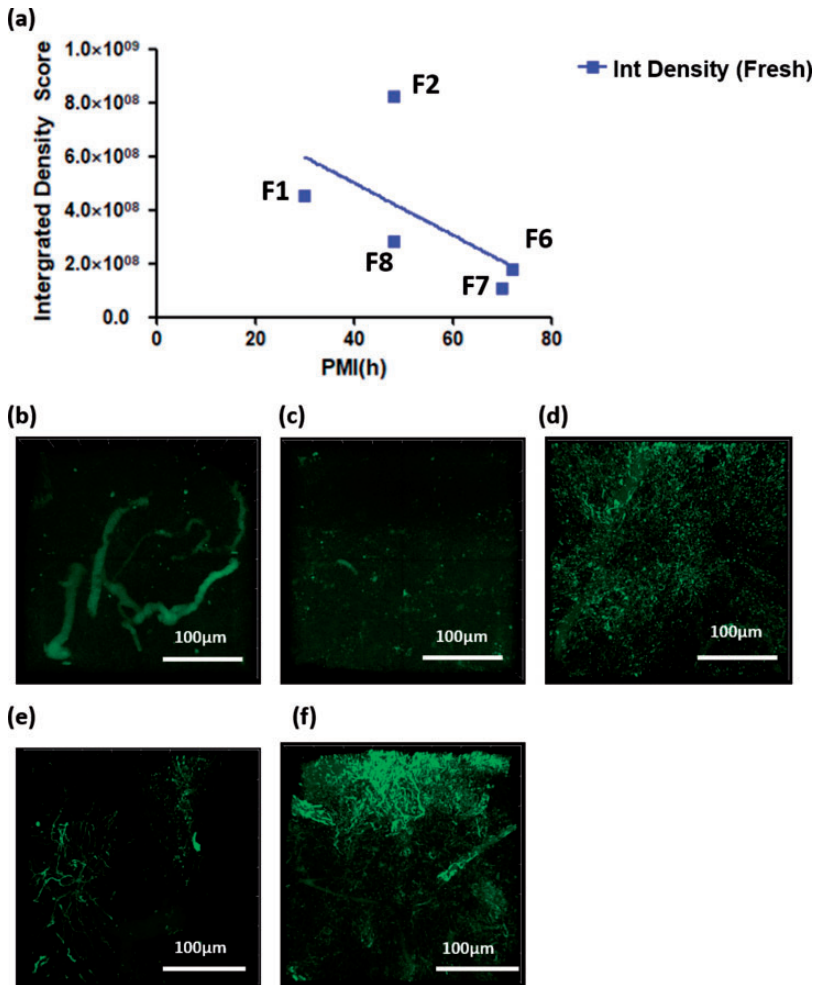


Figure 4. Amount of stained antigen (calculated as the “integrated density” score in ImageJ) plotted against the postmortem interval (PMI). (a) Linear plot ($r = r^2 0.3557$) and (b–f) three-dimensional images (view looking down the z-axis) of antigen-stained (b) F1, (c) F2, (d) F6, (e) F7, and (f) F8 after 4-day staining (green: glial fibrillary acidic protein).

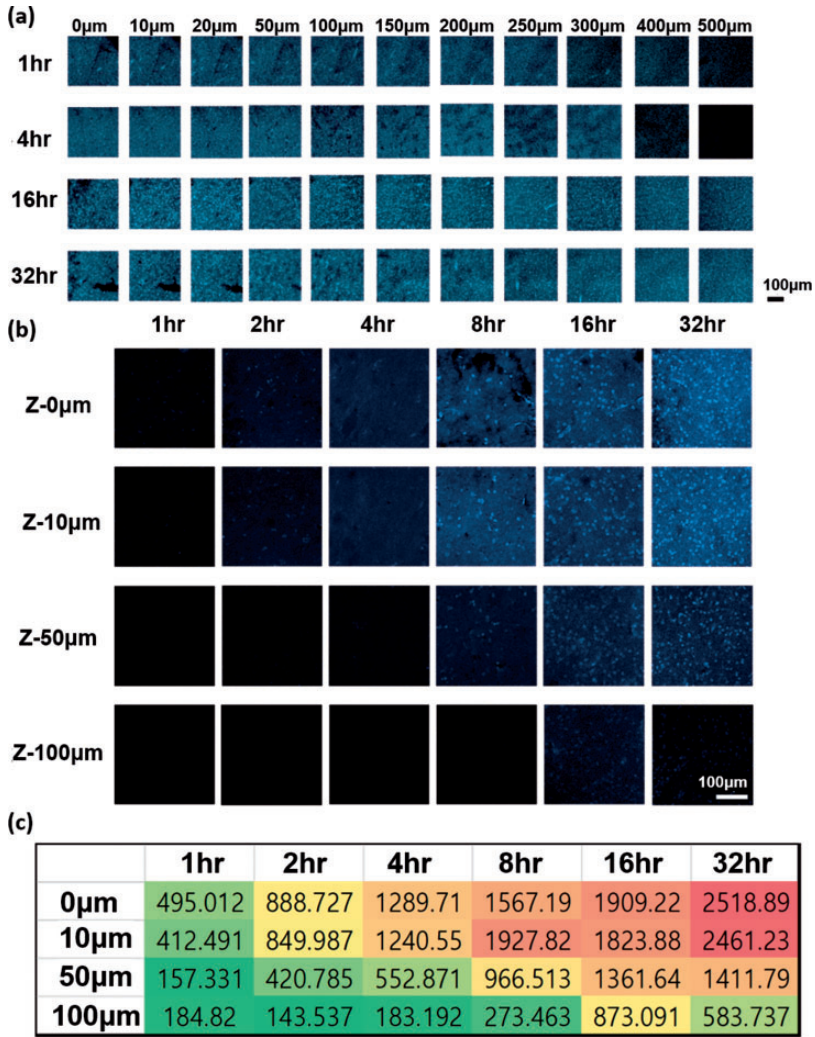


Figure 5. Penetration depth of 4',6-diamidino-2-phenylindole (DAPI) staining in the fresh human brain. (a) Results of DAPI staining set to the optimal values for each plane. (b) Results of DAPI staining set to the same values for each plane. (c) Heatmap of DAPI staining efficiency based on time and depth (the values in the heatmap are the integrated density [“IntDen”] values in ImageJ).

in depth between 4DS-C and 11DS and between 4DS and 11DS were not significant.

Visualizing the 3D macrostructure of the human brain

Using our tissue clearing technique, 4DS as the staining method, and lectin as the

staining dye, we were able to obtain an image of a blood vessel, including its intricate branching structure, up to a depth of approximately 800μm (Figure 7a, <https://photos.app.goo.gl/oMaLRxPuAWtgunjM7>). Furthermore, using 4DS as the staining method and anti-GFAP antibody, we were able to image a

Table 4. Summary of the three different staining methods.

Staining method	Blocking	Primary antibody	Washing	Secondary antibody	Washing
4-day incubation in PBS (4DS)	Donkey 3% + 0.01% Triton-X 4 hours	GFAP 1:500 + 4 days	PBS 2 days	Rabbit 488 1:500 DAPI 1:1000 (405) Lectin 1:500 (594) + 4 days	PBS 2 days
11-day incubation in PBS (11DS)	Donkey 3% + 0.01% Triton-X 4 hours	GFAP 1:500 + 11 days	PBS 2 days	Rabbit 488 1:500 DAPI 1:1000 (405) Lectin 1:500 (594) + 11 days	PBS 2 days
4-day incubation using DeepLabel kit (4DS-C)	Permeabilization buffer 1 day	GFAP 1:500 in anti-body dilution buffer + 4 days	PBS 2 days	Rabbit 488 1:500 DAPI 1:1000 (405) Lectin 1:500 (594) in antibody dilution buffer + 4 days	PBS 2 days

DAPI, 4',6-diamidino-2-phenylindole; GFAP, glial fibrillary acidic protein; PBS, phosphate-buffered solution.

Table 5. Comparison of the three staining methods.

Staining Method	4DS	11DS	4DS-C
Staining time for primary antibody (days)	4	11	4
Antibody penetration depth (mean) (µm)	65	125	160
Complexity	+	+	+
Tissue contamination	++	+++	+
Cost	+	+	++

Complexity was evaluated based on the number of steps in each protocol. Tissue contamination indicates the extent of visible artifacts after staining. Cost indicates the cost of the staining kit. +, low; ++, medium; +++, high. 4DS, 4-day staining; 4DS-C, 4-day staining with a commercial kit; 11DS, 11-day staining.

human brain astrocyte with an extremely complex structure (Figure 7b, <https://photos.app.goo.gl/Vd3rWxaks9uaDMje8>). Furthermore, using the 4DS method, a composite image of human brain astrocytes (from GFAP staining), nuclei (from DAPI staining), and blood vessels (from lectin staining) was created (Figure 7c, <https://photos.app.goo.gl/f4zMV5hMPqSEgRQy6>).

Discussion

In the current study, we presented a protocol for the optimal tissue clearing and staining of human brain samples. We found that fresh samples were more suitable than cadaver samples for use in tissue clearing experiments. We also determined that the DeepLabel Kit staining method was optimal in terms of staining time, antibody penetration depth, and level of method complexity.

To our knowledge, this is the first human brain clearing study to quantify and compare clearing and staining protocols. A recent study has reported on clearing methods for the human brain.¹⁹ Both our study and the previous study used fresh and cadaver samples. However, the previous

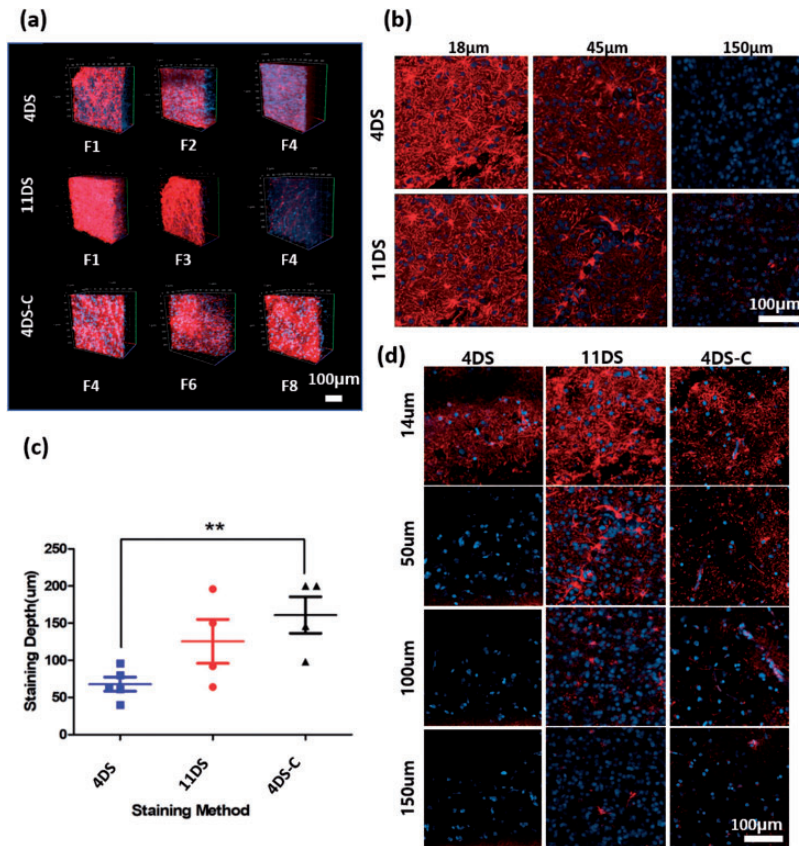


Figure 6. Comparison of the staining methods. (a) Images of fresh human brain samples (F1, F2, F3, F4, F6, F8). (b) Fresh sample (F2) staining results from 4-day staining (4DS) and 11-day staining (11DS) (red: glial fibrillary acidic protein [GFAP], blue: 4',6-diamidino-2-phenylindole [DAPI]). (c) GFAP antibody penetration depth according to the staining method. $**p < 0.01$. (d) Fresh sample (F4) staining results after 4DS, 11DS, and 4-day staining with a commercial kit (4DS-C) (red: GFAP, blue: DAPI). Samples F1 and F2 are the same as the samples shown in Figure 4.

study investigated staining methods for fresh and cadaver samples without including any quantification or direct comparisons between the sample types. Our study took this approach one step further by rigorously quantifying the time, depth, and efficiency of both antibody and chemical staining. In addition, whereas the previous study used only traditional buffers, we investigated various staining methods (traditional buffers, a commercial buffer kit, and an electrophoresis device) and provided technical comparisons. 4DS was selected as

a staining method because it produced satisfactory image quality at an affordable cost. However, there was no difference in tissue integrity between the 4DS- and 4DS-C-stained samples. Another difference is that we used X-CLARITYTM for tissue clearing, whereas the previous study used OPTiclear. Furthermore, an additional study has previously published methods on human tissue clearing, but did not quantify or compare these methods.² Our study had a much larger sample size compared with these previous studies (previous

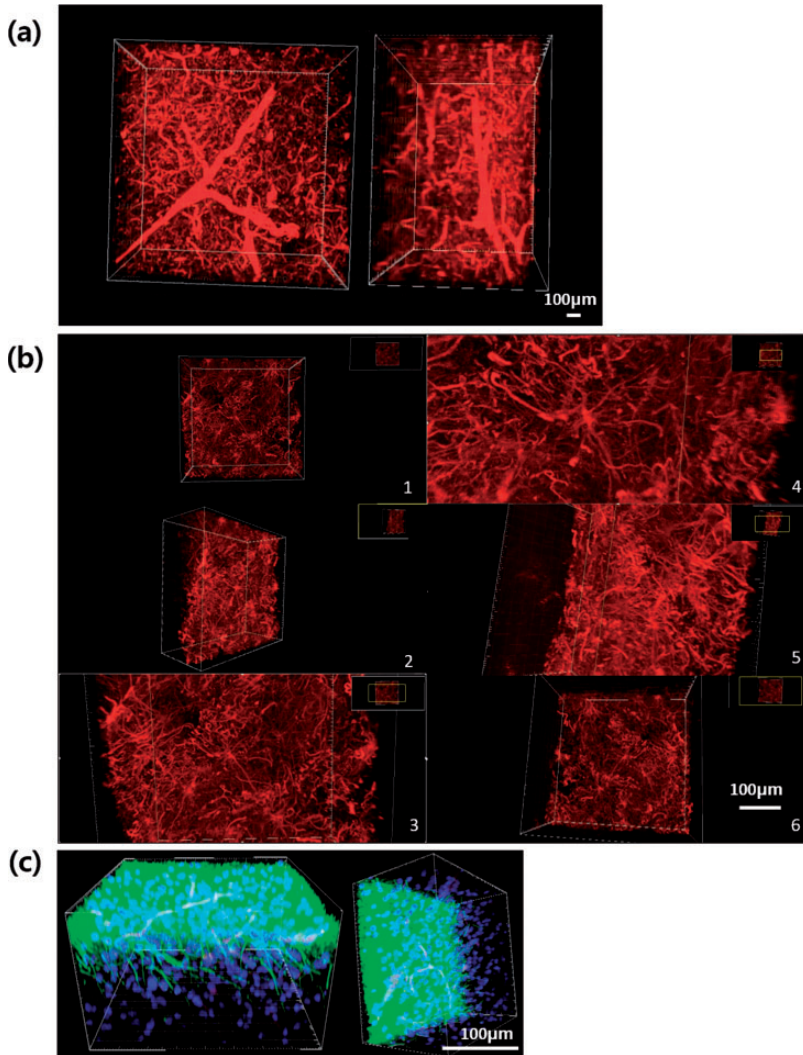


Figure 7. Visualizing the three-dimensional structure of the human brain. (a) Human blood vessel, (b) human astrocyte, and (c) structure of the human brain (red: lectin, green: glial fibrillary acidic protein, blue: 4',6-diamidino-2-phenylindole).

studies: 1–5 samples vs. our study: 15 samples). Additionally, whereas these previous studies used only biobank samples, we had access to fresh tissue samples and could therefore investigate the importance of fresh sample collection and preparation for the human clearing study. Last, considering the staining depth of 800 µm that was achieved, the present investigation

constitutes a large-scale successful human brain clearing and chemical staining study, although it is not the largest reported staining depth. In previous studies, brain samples were stained up to 4500 and 1500 µm in depth using Multiscale Architechtonic Staining of Human cortex (MASH) and OptiClear staining protocols, respectively.^{2,25} However, the aforementioned studies

required a longer time period for the whole procedure (10 days and 3.5 months, respectively) compared with our study (about 6 days).

We speculate that the differences in clearing efficiency between fresh and cadaver samples are related to fixation time. Cadaver samples underwent prolonged fixation (approximately 2 years) before tissue clearing, whereas fresh samples were fixed for just 1 week. This prolonged fixation time may cause excess crosslinking of molecules with methylene bridges, which might delay lipid removal during clearing. In addition, the fresh postmortem samples were preserved at 4°C before sample collection, which may cause tissue decay. However, gross tissue decay was not observed during sample collection. The difference in the opacity curve between fresh samples (F1, F2, and F3 vs. F4, F5, and F8) can be explained by the difference in sample thickness, which was mentioned in the methods.

Cadaver samples had more artifacts compared with fresh samples. The artifacts may result from autofluorescence or laser scattering phenomena. Although autofluorescence is assumed to be similar in both sample types, laser scattering phenomena are likely to occur more intensely in cadaver samples because of the increased crosslinking caused by a prolonged fixation time. Furthermore, differences in clearing efficiency were also related to differences in artifacts. When the clearing time was fixed, the cadaver samples were less cleared, and there were more artifacts in the cadaver samples because of their opacity. However, even when the clearing efficiency was the same between the two sample types, the cadaver samples continued to have more artifacts, likely because of the remaining brown/yellow tint following tissue clearing.^{2,19}

The greatest difference between the fresh and cadaver samples was in DAPI staining.

When the tissue was frozen, sectioned, and stained, DAPI staining was not observed in cadaver samples. The loss of DAPI staining was likely a result of the DNA degradation caused by either a long fixation time or a long interval between the time of death and the tissue collection time. Because DNA is fairly stable, it is likely to be the former option. However, a previous study has reported the successful staining of cadaver samples with DAPI;² therefore, the staining of cadaver samples with DAPI does not seem to be a universal problem, and may be related to tissue collection procedures that are unique to our university. It is difficult for researchers to participate in the fixation procedures of cadaver samples because samples are obtained according to the procedure stated by the donor body of research. Thus, the time period from death to fixation varies. Whereas fresh samples were harvested within 48–80 hours, cadaver samples may have been harvested more than 80 hours postmortem.

With regard to antibody staining, both fresh and cadaver samples had a similar pattern and depth of GFAP staining, with slight (but insignificant) differences in the amount of antigen. These may have been caused by formaldehyde protein crosslinks hindering antibody binding in cadaver samples.²⁶ Staining quantity is determined by antigen quantity, antigen quality, antibody penetration, and antibody–antigen affinity, among other qualities. A longer PMI may result in protein degradation and bacterial decomposition, causing a decrease in antigen quantity and quality. Thus, based on our results, human brain samples with a PMI of over 60 hours are not recommended for immunohistochemical staining.

This study has some limitations. First, although we succeeded in imaging GFAP staining in 3D, anti-NeuN and anti-neurofilament antibodies did not work in cleared human brain samples. This may be because of antibody-specific heterogeneity

regarding staining protocols, and needs to be investigated in future studies. Second, all of our results were restricted to small samples of the cortex; thus, our protocol cannot be generalized to other parts of the human brain. Third, our sample number for some of the staining techniques was too small to test for statistical significance. Last, the images were mostly acquired in the 20× objective because of limited microscope resolution and astrocyte morphology. Although 10× objective images were not presented in this paper because of their low image quality, they showed staining penetration to a deeper extent compared with the 20× objective images.

In conclusion, we successfully visualized 3D macrostructure in the human brain using an optimized clearing and staining method. This protocol requires fresh human brain tissue and the use of the DeepLabel staining kit to produce the best results. This optimized method will open new avenues for disease diagnosis and human brain research.

Declaration of conflicting interests

The authors declare that there is no conflict of interest.

Funding

The authors disclosed receipt of the following financial support for the research, authorship, and/or publication of this article: This work was supported by the National Research Foundation of Korea (NRF), and a grant funded by the Korean Government (No. 2016R1D1A1B03932985, NRF-2018R1A5A2025964). This work was also supported by the Creative-Pioneering Researchers Program through Seoul National University.

ORCID iDs

Jang Ho Ahn  <https://orcid.org/0000-0003-1058-812X>

Hyung Jin Choi  <https://orcid.org/0000-0003-0593-6978>

References

1. Chung K and Deisseroth K. CLARITY for mapping the nervous system. *Nat Methods* 2013; 10: 508–513. DOI: 10.1038/nmeth.2481.
2. Lai HM, Liu AKL, Ng HHM, et al. Next generation histology methods for three-dimensional imaging of fresh and archival human brain tissues. *Nat Commun* 2018; 9: 1066. DOI: 10.1038/s41467-018-03359-w.
3. Harrison CH, Buckland GR, Brooks SE, et al. A novel method to visualise the three-dimensional organisation of the human cerebral cortical vasculature. *J Anat* 2018; 232: 1025–1030. DOI: 10.1111/joa.12805.
4. Fowler JL, Lee SS, Wesner ZC, et al. Three-dimensional analysis of the human pancreas. *Endocrinology* 2018; 159: 1393–1400. DOI: 10.1210/en.2017-03076.
5. Azaripour A, Lagerweij T, Scharfbillig C, et al. Three-dimensional histochemistry and imaging of human gingiva. *Sci Rep* 2018; 8: 1647. DOI: 10.1038/s41598-018-19685-4.
6. Tinne N, Antonopoulos GC, Mohebbi S, et al. Three-dimensional hard and soft tissue imaging of the human cochlea by scanning laser optical tomography (SLOT). *PLoS One* 2017; 12: e0184069. DOI: 10.1371/journal.pone.0184069.
7. Vigouroux RJ, Belle M and Chédotal A. Neuroscience in the third dimension: shedding new light on the brain with tissue clearing. *Mol Brain* 2017; 10: 33. DOI: 10.1186/s13041-017-0314-y.
8. Hama H, Hioki H, Namiki K, et al. ScaleS: an optical clearing palette for biological imaging. *Nat Neurosci* 2015; 18: 1518–1529. DOI: 10.1038/nn.4107.
9. Yang B, Treweek JB, Kulkarni RP, et al. Single-cell phenotyping within transparent intact tissue through whole-body clearing. *Cell* 2014; 158: 945–958. DOI: 10.1016/j.cell.2014.07.017.
10. Nojima S, Susaki EA, Yoshida K, et al. CUBIC pathology: three-dimensional imaging for pathological diagnosis. *Sci Rep* 2017; 7: 9269. DOI: 10.1038/s41598-017-09117-0.
11. Kirst C, Skriabine S, Vieites-Prado A, et al. Mapping the fine-scale organization and

- plasticity of the brain vasculature. *Cell* 2020; 180: 780–795.e25. DOI: 10.1016/j.cell.2020.01.028.
12. Qi Y, Yu T, Xu J, et al. FDISCO: advanced solvent-based clearing method for imaging whole organs. *Sci Adv* 2019; 5: eaau8355. DOI: 10.1126/sciadv.aau8355.
 13. Zhu J, Yu T, Li Y, et al. MACS: rapid aqueous clearing system for 3D mapping of intact organs. *Adv Sci (Weinh)* 2020; 7: 1903185. DOI: 10.1002/advs.201903185.
 14. Chung K, Wallace J, Kim SY, et al. Structural and molecular interrogation of intact biological systems. *Nature* 2013; 497: 332–337. DOI: 10.1038/nature12107.
 15. Ueda HR, Ertürk A, Chung K, et al. Tissue clearing and its applications in neuroscience. *Nat Rev Neurosci* 2020; 21: 61–79. DOI: 10.1038/s41583-019-0250-1.
 16. Costantini I, Cicchi R, Silvestri L, et al. In-vivo and ex-vivo optical clearing methods for biological tissues: review. *Biomed Opt Express* 2019; 10: 5251–5267. DOI: 10.1364/BOE.10.005251.
 17. Costantini I, Ghobril JP, Di Giovanna AP, et al. A versatile clearing agent for multi-modal brain imaging. *Sci Rep* 2015; 5: 9808. DOI: 10.1038/srep09808.
 18. Ando K, Laborde Q, Lazar A, et al. Inside Alzheimer brain with CLARITY: senile plaques, neurofibrillary tangles and axons in 3-D. *Acta Neuropathol* 2014; 128: 457–459. DOI: 10.1007/s00401-014-1322-y.
 19. Liu AK, Hurry ME, Ng OT, et al. Bringing CLARITY to the human brain: visualization of Lewy pathology in three dimensions. *Neuropathol Appl Neurobiol* 2016; 42: 573–587. DOI: 10.1111/nan.12293.
 20. Ando K, Laborde Q, Brion JP, et al. Chapter 21–3D imaging in the postmortem human brain with CLARITY and CUBIC. In: Huitinga I and Webster MJ (eds) *Handbook of Clinical Neurology*. Amsterdam: Elsevier, 2018, pp.303–317.
 21. Phillips J, Laude A, Lightowers R, et al. Development of passive CLARITY and immunofluorescent labelling of multiple proteins in human cerebellum: understanding mechanisms of neurodegeneration in mitochondrial disease. *Sci Rep* 2016; 6: 26013. DOI: 10.1038/srep26013.
 22. Morawski M, Kirilina E, Scherf N, et al. Developing 3D microscopy with CLARITY on human brain tissue: towards a tool for informing and validating MRI-based histology. *Neuroimage* 2018; 182: 417–428. DOI: 10.1016/j.neuroimage.2017.11.060.
 23. Zhao S, Todorov MI, Cai R, et al. Cellular and molecular probing of intact human organs. *Cell* 2020; 180: 796–812.e19. DOI: 10.1016/j.cell.2020.01.030.
 24. Lee E, Choi J, Jo Y, et al. ACT-PRESTO: rapid and consistent tissue clearing and labeling method for 3-dimensional (3D) imaging. *Sci Rep* 2016; 6: 18631. DOI: 10.1038/srep18631.
 25. Hildebrand S, Schueth A, Herrler A, et al. Scalable labeling for cytoarchitectonic characterization of large optically cleared human neocortex samples. *Sci Rep* 2019; 9: 10880. DOI: 10.1038/s41598-019-47336-9.
 26. Fowler CB, Cunningham RE, Waybright TJ, et al. Elevated hydrostatic pressure promotes protein recovery from formalin-fixed, paraffin-embedded tissue surrogates. *Lab Invest* 2008; 88: 185–195. DOI: 10.1038/labinvest.3700708.